J Mol Model (2014) 20:2502
DOI 10.1007/s00894-014-2502-3

ORIGINAL PAPER

# Understanding the effects of the number of pyrazines and their positions on charge-transport properties in silylethynylated *N*-heteropentacenes

**Shou-Feng Zhang · Xian-Kai Chen · Jian-Xun Fan · Jing-Fu Guo · Ai-Min Ren · Yu-Wei Li**

Received: 14 May 2014 / Accepted: 13 October 2014 / Published online: 5 November 2014


**Abstract** The charge-transport properties of a series of silylethynylated *N*-heteropentacenes (TIPS-PEN-*x*N; $x = 2, 4$) were systematically investigated using Marcus electron-transfer theory coupled with kinetic Monte Carlo simulations. Electronic structure calculations showed that introducing more pyrazine rings decreases the energy levels of the lowest unoccupied molecular orbitals (LUMOs) and should aid electron transfer. The number and the positions of the pyrazine rings greatly influence the molecular packing in crystals and hence the intermolecular electronic coupling. Furthermore, the introduction of internal (rather than external) pyrazine rings leads to a better charge-transport network. Transport parameters evaluated from the hopping and band-like models both demonstrate that, among the TIPS-PEN-*x*N molecules, B-TIPS-PEN-4N—which has two internal pyrazine rings—is the most promising n-type material.

**Keywords** Organic semiconductors · *n*-type materials · Effective mass · Hopping and band-like mechanisms · Dynamic disorder

Both S.-F. Zhang and X.-K. Chen are the first authors and they contributed to this paper equally.

**Electronic supplementary material** The online version of this article (doi:10.1007/s00894-014-2502-3) contains supplementary material, which is available to authorized users.

S.-F. Zhang · X.-K. Chen · J.-X. Fan · A.-M. Ren (✉)
State Key Laboratory of Theoretical and Computational Chemistry, Institute of Theoretical Chemistry, Jilin University, Changchun 130023, China
e-mail: aimin_ren@yahoo.com

J.-F. Guo
School of Physics, Northeast Normal University, Changchun 130024, People's Republic of China

Y.-W. Li
State Key Laboratory of Superhard Materials, Jilin University, Changchun 130012, China

## Introduction

Organic semiconductors have drawn much attention due to their potential applications in low-cost, large-area, and flexible electronic devices, such as organic light-emitting diodes (OLEDs) [1, 2], organic field-effect transistors (OFETs) [3–5], solar cells [6, 7], and sensors [8–11]. Significant progress has been made so far in p-channel organic semiconductor development [12–20]. Some representative p-type materials have surpassed amorphous silicon devices, with hole mobilities of >10 $cm^2\ V^{-1}\ s^{-1}$ observed at room temperature (in pentacene, rubrene, and so on) [12, 21, 22]. In contrast, the progress of n-type materials has lagged behind somewhat due to the high injection energy barrier for electrons and the poor stability of organic radical anions in the ambient atmosphere. Considering that complementary integrated circuits consisting of both p-type and n-type transistors can achieve far greater speed, reliability, and stability than unipolar circuits [23, 24], the molecular design and synthesis of excellent n-type organic semiconducting materials is urgently required.

Among various approaches to n-type material development, the introduction of pyrazine rings into oligoacenes has been found to be a successful strategy. In terms of experimental studies, Yamashita and co-workers were the first to report n-type OFETs based on pyrazinoacene-type molecules, and they found that introducing pyrazine rings increased the electron affinity (EA), leading to higher electron mobilities [25, 26]. Zhu et al. demonstrated that molecules with larger fused-ring pyrazine cores exhibited lower LUMO energies and relatively low reorganization energies [27]. Miao's group reported a series of OFETs based on *N*-heteropentacenes with electron mobilities that could reach as high as 3.3 $cm^2\ V^{-1}\ s^{-1}$, meaning that they rank among the best-performing n-type materials [28–30]. In terms of theoretical studies, Chao et al. performed a detailed investigation of N-functionalized pentacenes, and their computational calculations indicated

that N atoms reduced the influence of $\lambda$ (the reorganization energy) on functionalization and afforded a larger window for tuning HOMO (highest occupied molecular orbital)/LUMO energies. Moreover, N atoms also provided the opportunity to promote $\pi$-stacking crystal structures via C–H···N interactions [31]. Winkler's group predicted that introducing more nitrogen atoms into pentacene would increase the EA and hence aid electron transfer [32]. In our previous work, we studied the transport properties of typical materials with pyrazine rings from the perspective of the molecular stacking motif, carrier mobilities, and electronic band structures. The results showed that introducing pyrazine can lead to excellent n-type OFET materials due to the small electron reorganization energies and large electronic couplings associated with the $\pi$-stacking structures [33].

However, one crucial question that is still to be answered comprehensively is: how do the number of pyrazines and their positions influence the charge-transport properties? For example, while the isomers 1,4,8,11-tetraaza-6,13-pentacenequinone (TA-PEN-1 in Fig. 1a) and 5,7,12,14-tetraaza-6,13-pentacenequinone (TA-PEN-2 in Fig. 1a) show similar molecular packing structures, the latter exhibits three orders of magnitude higher experimental electron mobility values (0.05–0.12 $cm^2\ V^{-1}\ s^{-1}$) than the former (2–6 × $10^{-5}$ $cm^2\ V^{-1}\ s^{-1}$) [34, 35]. However, recent theoretical work reported by the Zhao group found that the predicted electron mobility of TA-PEN-1 (8.75 $cm^2\ V^{-1}\ s^{-1}$) is much higher than that of TA-PEN-2 (1.54 $cm^2\ V^{-1}\ s^{-1}$). This discrepancy was attributed to the amorphous films of TA-PEN-1, based on an analysis of experimental X-ray diffraction patterns [36]. Therefore, it is still hard to pinpoint which position of pyrazine is the most beneficial to electron transport in these two TA-PEN (tetraaza-6,13-pentacenequinone) molecules, and the effect of the position of pyrazine on the charge transport properties should be studied for other *N*-heteropentacenes. Aside from the optimal position of pyrazine, the effect of the number of pyrazines present on the electron mobility is also not clear [37]. For *N*-heteropentacenes based on 6,13-bis(triisopropylsilylethynyl)pentacene (TIPS-PEN) [38], the electron mobility of B-TIPS-PEN-2N with one pyrazine was found to be as low as $10^{-4}$ $cm^2\ V^{-1}\ s^{-1}$, but it reached 3.3 $cm^2\ V^{-1}\ s^{-1}$ for B-TIPS-PEN-4N with two pyrazine rings [29]. The question here is: why does the presence of only one extra pyrazine have such a marked effect on the electron mobility? To get answers to these questions, the effects of the number of pyrazines and their positions on the charge-transport properties of the system must be investigated.

In the work reported in the present paper, we selected four *N*-heteropentacenes based on TIPS-PEN to study (see Fig. 1b). These *N*-heteropentacenes varied in both the number and the positions of the pyrazine rings in the *N*-heteropentacene, so they provided the opportunity to comprehensively study the influence of the pyrazine rings on the charge-transport properties of *N*-heteropentacenes. This paper is arranged as follows. The next section briefly presents the theoretical and computational methods used in the present work. The "Results and discussion" section explores the effect of the number and the positions of pyrazines on the charge-transport parameters in both the hopping mechanism and the band-like mechanism. The effect of dynamic disorder on the carrier mobilities of these *N*-heteropentacenes is also discussed in this section. The final section of the paper provides some concluding remarks about the results.

## Theoretical and computational methods

In general, there are two types of charge-transport mechanisms in organic semiconductor materials: an incoherent hopping mechanism [39–43] and a coherent band mechanism [22, 44–47]. However, it is still challenge to classify the charge-transport behavior of an organic semiconductor into a hopping or a band-like mechanism. In this study, both mechanisms were taken into consideration.

For the hopping mechanism, each hopping event can be described as a charge-transport process that follows the

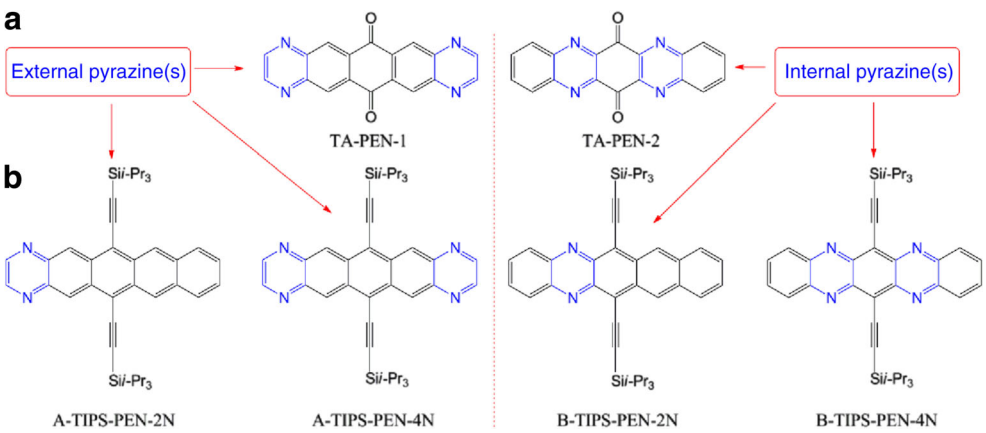


**Fig. 1** (*a*) Chemical structures of 1,4,8,11-tetraaza-6,13-pentacenequinone and 5,7,12,14-tetraaza-6,13-pentacenequinone. (*b*) Chemical structures of the four silylethynylated *N*-heteropentacenes investigated in this study

reaction: $M+M^{+/-}=M^{+/-}+M$. According to the Marcus electron transfer theory, the charge transfer rate ($k$) can be expressed as [48]

$$k_{ct} = \frac{t^2}{\hbar}\sqrt{\frac{\pi}{\lambda k_B T}}\exp\left\{-\frac{\lambda}{4k_B T}\right\}. \quad (1)$$

There are two key parameters in hopping charge transport: the reorganization energy ($\lambda$) and the transfer integral ($t$). The adiabatic potential energy method can be applied to calculate $\lambda$. The internal reorganization energies for holes ($\lambda_h$) and electrons ($\lambda_e$) are then given by

$$\lambda_h = \mathrm{VIP}-\mathrm{HEP} = [E(M^+)-E(M)]-[E^+(M^+)-E^+(M)] \quad (2)$$

$$\lambda_e = \mathrm{EEP}-\mathrm{VEA} = [E^-(M)-E^-(M^-)]-[E(M)-E(M^-)]. \quad (3)$$

Here, VIP and VEA refer to the vertical ionization potential and electron affinity, while HEP and EEP are the hole and electron extraction potentials, respectively. In addition, $E^{+/-}(M)$ is the energy of the neutral molecule at the optimized ion geometry, $E^{+/-}(M^{+/-})$ is the energy of the ionized state at the optimized neutral molecular geometry, and $E(M)$ and $E(M^{+/-})$ are the ground-state energies of the neutral and charged molecular states, respectively. All neutral and ionic geometries were optimized at the density functional theory (DFT) level with the B3LYP functional [49–51] and the 6-31G(d,p) basis set [52–54], using the Gaussian09 software package [55]. To accurately characterize the energies of these species, the 6-31++G(d,p) basis set was applied to perform single-point calculations on the optimized geometric structures.

Transfer integrals of nearest-neighboring dimers were calculated based on the fragment orbital approach using the following expression [56–58]:

$$t_{ij} = \frac{H_{ij}-S_{ij}\left(e_{ii}+e_{jj}\right)/2}{1-S^2_{ij}}, \quad (4)$$

where the charge transfer integral $H_{ij}=\langle\varphi_i|H|\varphi_j\rangle$, the site energies $e_{ii}=\langle\varphi_i|H|\varphi_i\rangle$ and $e_{jj}=\langle\varphi_j|H|\varphi_j\rangle$, and the spatial overlap $S_{ij}=\langle\varphi_i|\varphi_j\rangle$, respectively. Here, $\varphi_{i/j}$ is the HOMO/LUMO (for the hole/electron transport process, respectively) following Löwdin's symmetric transformation of one monomer, which can be used as the orthogonal basis set in the calculations, and $H$ is the Kohn–Sham Hamiltonian of the dimer system. All transfer integral calculations were performed using the Amsterdam Density Functional (ADF) program package and the PW91/TZ2P method [59].

The hopping carrier mobility ($\mu$) can be expressed by the Einstein equation

$$\mu = \frac{e}{K_B T}D. \quad (5)$$

Here, $e$ refers to the electronic charge, $T$ is the temperature, $K_B$ is Boltzmann's constant, and $D$ is the charge diffusion coefficient. The charge diffusion coefficient can be obtained via the Brownian motion model and kinetic Monte Carlo (KMC) simulation technology by the following equation [60–65]:

$$D = \lim_{t\to\infty}\frac{1}{2n}\frac{\left\langle x^2(t')\right\rangle}{t'}, \quad (6)$$

where $n$ is the dimensionality and $t'$ is the simulation time.

For comparison purposes, the relevant transport parameters in the band-like mechanism were also calculated. The electronic band structure was calculated using the Perdew–Burke–Ernzerhof (PBE) exchange-correlation functional [66] and the plane-wave basis set in the Vienna ab initio simulation package (VASP) [67–69]. Electron–ion interactions were described using the projector augmented wave (PAW) potentials [70, 71]. The kinetic energy cutoff for the wave function expansion was set to 650 eV. An 8×8×8, 5×5×5, 8×8×8, 6×6×6 Monkhorst-Pack $k$-point mesh [72] was employed for each crystal Brillouin zone, respectively. The inverse effective mass tensor can be defined as

$$\frac{1}{m_{ij}} = \frac{1}{\hbar^2}\frac{\partial^2 E}{\partial k_i \partial k_j}, \quad (7)$$

where $E$ is the band energy, $\hbar$ is the Planck constant, and $k_{i/j}$ is the electron wave vector for the Cartesian coordinates $i/j$ in reciprocal space, respectively. Sperling's centered difference method with d$k$ = 0.01/bohr was used for effective mass calculations [73–75].

## Results and discussion

### HOMO/LUMO energies, IPs, and EAs

A detailed analysis of the electronic structures of the molecules of interest is needed to clarify the origin of the observed differences in their charge transport properties. On the one hand, the relative magnitudes of the HOMO and LUMO energies can provide a qualitative indication of the capacity for hole and electron injection, respectively [76]. When the interfacial vacuum energy shift is negligible, the height of the energy barrier to hole/electron injection, which is usually treated as a Mott–Schottky barrier, can be defined as the energy difference between the electrode's work function ($\Phi_m$) and the HOMO/LUMO energy level of the organic semiconducting material: $\Phi_B=|\mathrm{HOMO}|-\Phi_m$ for hole injection and $\Phi_B=\Phi_m-|\mathrm{LUMO}|$ for electron injection, respectively [23, 77]. Therefore, we would expect the work function for the metal electrode to be close to the HOMO/LUMO energy level, leading to a low energy barrier to injection and hence good

performance with a high carrier mobility. On the other hand, semiconductor materials can easily interact with water or oxygen due to the strong reducing ability of the organic radical anions formed during the charge-transport process. Therefore, it is important to note that a high electron affinity (EA) is required for an n-type semiconductor material in order to reduce its sensitivity to oxidants and hence improve environmental stability.

For a good n-type semiconducting material, a high electron affinity is a key to the stability of radical anions in the ambient atmosphere. In general, an n-type material needs to have an electron affinity of at least 3 eV to observe n-channel behavior, and it should not be much larger than 4 eV to avoid overly compromising its stability [5, 23]. The vertical and adiabatic electron affinities (VEA/AEA) and ionization potentials (VIP/AIP) for the four *N*-heteropentacenes as well as TIPS-PEN were calculated and are listed in Table 1. Compared to the parent molecule, chemical derivatives containing pyrazine rings possess larger EAs (VEA: 2.2~2.66 eV; AEA: 2.29~2.76 eV) and IPs (VIP: 6.21~6.65 eV; AIP: 6.12~6.54 eV). Introducing pyrazine rings will undoubtedly significantly improve the stability of the electron-transport process in these semiconducting materials. Also, molecules with two pyrazine rings show higher EAs than molecules with one pyrazine, which implies that introducing more pyrazine rings enhances the environmental stability of n-type materials. When considering the effect on the molecular stability of positioning the rings externally or internally, it was found that molecules containing internal pyrazine rings exhibited larger EAs than molecules containing external pyrazine rings. This fact implies that the former yields more stable organic radical anions. To explain this, the contributions of the pyrazine ring to the LUMOs of A-TIPS-PEN-2N and B-TIPS-PEN-2N are shown in Fig. 2. Compared to the contribution of the benzene rings in TIPS-PEN, the contribution of the pyrazine ring to the LUMO is significantly greater, and the contribution of an internal pyrazine ring (29.2 %) to the LUMO is larger than that of an external pyrazine ring (21.6 %). This clearly indicates that an internal pyrazine ring has stronger electron-withdrawing ability than an external pyrazine does, so the molecule B-TIPS-PEN-2N presents a lower LUMO energy and a higher electron affinity than the molecule A-TIPS-PEN-2N. This explanation also holds for molecules containing two internal/external pyrazine rings.

The HOMO and LUMO energies for all *N*-heteropentacenes as well as TIPS-PEN are also listed in Table 1. First, it is apparent that the HOMO/LUMO levels for silylethynylated *N*-heteropentacenes are all lower than those of TIPS-PEN, and they all have similar energy gaps of about 1.85 eV. From a charge-transfer viewpoint, the lower LUMO levels should aid electron injection. Thus, the successful conversion of p-type TIPS-PEN to n-type semiconducting materials can be credited to some extent to the lower LUMO energies induced by the introduction of pyrazine rings. Second, it is also apparent that the LUMO levels of the molecules A-TIPS-PEN-4N and B-TIPS-PEN-4N are lower than those of the molecules A-TIPS-PEN-2N and B-TIPS-PEN-2N. This indicates that introducing more pyrazine rings into the molecule will further reduce the LUMO energy, hence lowering the injection energy barrier. For instance, when a gold electrode (work function $\Phi_m = 5.1$ eV) is used for charge-carrier injection, the electron injection energy barrier heights increase in the order B-TIPS-PEN-4N ($\Phi_B = 1.33$ eV)<A-TIPS-PEN-4N ($\Phi_B = 1.58$ eV)<B-TIPS-PEN-2N ($\Phi_B = 1.67$ eV)<A-TIPS-PEN-2N ($\Phi_B = 1.83$ eV). The result also clearly demonstrates that introducing internal pyrazine rings is more beneficial to electron injection than introducing external rings. This can be explained as follows. Internal pyrazine rings contribute more to the LUMO than external pyrazine rings do. Therefore, in terms of influence on the electron distribution of the molecule, the benzene-pyrazine structure present inside a molecule with internal pyrazines exerts a greater influence on the electron distribution than the core acene structure present inside a molecule with external pyrazines does.

## Reorganization energies, transfer integrals, and carrier mobilities

Small reorganization energies and large intermolecular transfer integrals help to enhance the carrier mobility [78]. These two key factors can be calculated by considering a single molecule and neighboring dimers in the crystal, respectively.

**Table 1** HOMO/LUMO energies, energy gaps, vertical and adiabatic ionization potentials (VIP/AIP), and electron affinities (VEA/AEA) of the studied molecules. All values are in eV

| | $E_{HOMO}$ | $E_{LUMO}$ | $E_g$ | VIP | AIP | VEA | AEA |
|---|---|---|---|---|---|---|---|
| TIPS-PEN | −4.63 | −2.74 | 1.89 | 5.97 | 5.90 | 1.94 | 2.03 |
| A-TIPS-PEN-2N | −5.11 | −3.27 | 1.84 | 6.21 | 6.12 | 2.20 | 2.29 |
| A-TIPS-PEN-4N | −5.37 | −3.52 | 1.86 | 6.47 | 6.38 | 2.42 | 2.51 |
| B-TIPS-PEN-2N[a] | −5.23 | −3.43 | 1.80 | 6.31 | 6.22 | 2.33 | 2.42 |
| B-TIPS-PEN-4N[a] | −5.58 | −3.77 | 1.81 | 6.65 | 6.54 | 2.66 | 2.76 |

[a] Data from [33]

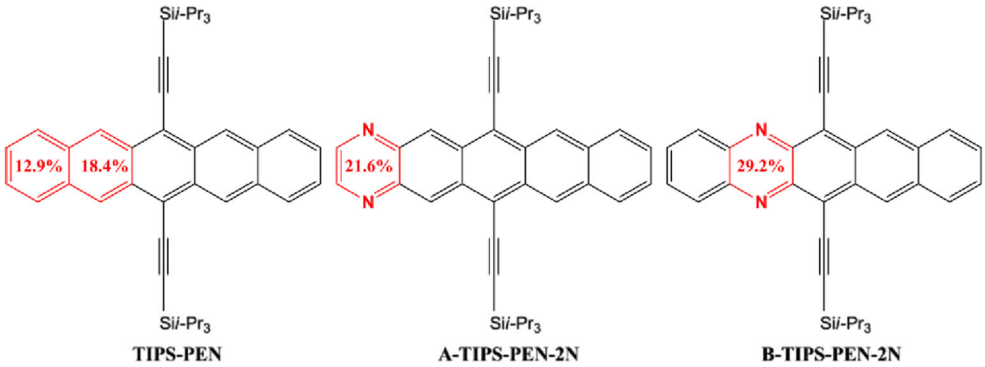


**Fig. 2** Contributions (%) of pyrazine to the LUMOs of TIPS-PEN, A-TIPS-PEN-2N, and B-TIPS-PEN-2N

An organic single crystal is an excellent model to use to elicidate intrinsic charge-transport properties because of the favorable conditions present, such as unlimited grain boundaries, an ordered structure, no traps, etc. To study the effect of introducing pyrazine rings into each silylethynylated *N*-heteropentacene on its charge-transport properties, it is very useful to explore the crystal structures of these molecules. The relevant detailed crystallographic data obtained from the Cambridge Structural Database are listed in Table 2. It can be seen that the crystal parameters of A-TIPS-PEN-2N, B-TIPS-PEN-2N, and B-TIPS-PEN-4N are very similar to those of TIPS-PEN. The only significant difference is the change of space group (SG): the space group of TIPS-PEN is *P*-1, whereas it is *P*1 for A-TIPS-PEN-2N and B-TIPS-PEN-2N. It is well known that the unit cells associated with space groups *P*-1 and *P*1 contain only one molecule, and that this molecule is symmetrical for *P*-1 and asymmetrical for *P*1. However, the lattice parameters of the A-TIPS-PEN-4N crystal are totally different from those of TIPS-PEN and the other silylethynylated *N*-heteropentacenes: the cell volume increases substantially to hold four single molecules, the space group changes to P21/c, and the crystal symmetry is more complicated. The molecular packing should be highly sensitive to weak intermolecular interactions, including electrostatic, exchange, induction, and dispersion interaction energies, etc. To investigate the nature of the intermolecular interactions in these *N*-heteropentacenes, symmetry-adapted perturbation theory (SAPT) was applied to calculate the noncovalent interaction between the face-to-face dimers, using the jun-cc-pVDZ basis set [79, 80].

For convenience, the SAPT energy was defined as the simplest truncated form ($E_{SAPT0}$), which is the summation of the electrostatic ($E_{elst}$), exchange ($E_{exch}$), induction ($E_{ind}$), and dispersion ($E_{disp}$) terms. Here, $E_{elst}=E^{(10)}_{elst}$, $E_{exch}=E^{(10)}_{exch}$, $E_{ind}=E^{(20)}_{ind,resp}+E^{(20)}_{exch\text{-}ind,resp}$, and $E_{disp}=E^{(20)}_{disp,resp}+E^{(20)}_{exch\text{-}disp,resp}$, respectively. $E^{(mn)}$ refers to the order in the perturbative expansion of the interaction potential and in fluctuation potential; "resp" indicates that orbital relaxation effects are included. As shown in Fig. 3, the displacement along the *x*-axis has a remarkable effect on the intermolecular interactions. Taking pair 1 in A-TIPS-PEN-2N as an example, the most attractive contribution between the two monomers is the dispersion force, and the strength of this dispersion force continually weakens as the displacement increases. The variation in $E_{SAPT0}$ with displacement for all four *N*-heteropentacenes is shown in Fig. 3. For molecules with external pyrazines, the largest $E_{SAPT0}$ occurs for a displacement of about half a pyrazine ring. However, for molecules with internal pyrazines, the largest $E_{SAPT0}$ occurs when the displacement is about one and a half pyrazine rings. This difference can be explained by the charge contribution, which will be discussed for the head-to-tail case. It was also found that molecules with two pyrazines show stronger intermolecular interactions than molecules with one pyrazine at the same displacement. That means that introducing two pyrazines will lead to a greater reduction in crystal lattice energy and will therefore yield greater lattice stability.

Aside from face-to-face van der Waals forces, there are also important weak intermolecular interactions between the monomers in head-to-tail dimers. The electrostatic potential (ESP) is an important influence on atomic or molecular behavior. Contour maps of ESP for all molecules are plotted in Fig. 4. As shown in the figure, the very negative electrostatic potential (red areas) is concentrated on the nitrogen atoms of

**Table 2** Lattice parameters (*a*, *b*, *c*, in Å; $\alpha$, $\beta$, $\gamma$, in degrees) and space groups (SG) for the unit cells of the systems studied

| System | *a* | *b* | *c* | $\alpha$ | $\beta$ | $\gamma$ | SG |
|---|---|---|---|---|---|---|---|
| TIPS-PEN [38] | 7.56 | 7.75 | 16.84 | 89.15 | 78.42 | 83.63 | *P*-1 |
| A-TIPS-PEN-2N [29] | 7.57 | 7.95 | 16.86 | 78.24 | 89.30 | 79.54 | *P*1 |
| A-TIPS-PEN-4N [29] | 13.75 | 18.90 | 14.84 | 90.00 | 99.37 | 90.00 | *P*21/*c* |
| B-TIPS-PEN-2N [30] | 7.66 | 7.72 | 16.98 | 78.23 | 88.76 | 81.78 | *P*1 |
| B-TIPS-PEN-4N [30] | 7.58 | 7.61 | 16.83 | 78.98 | 89.54 | 81.90 | *P*-1 |

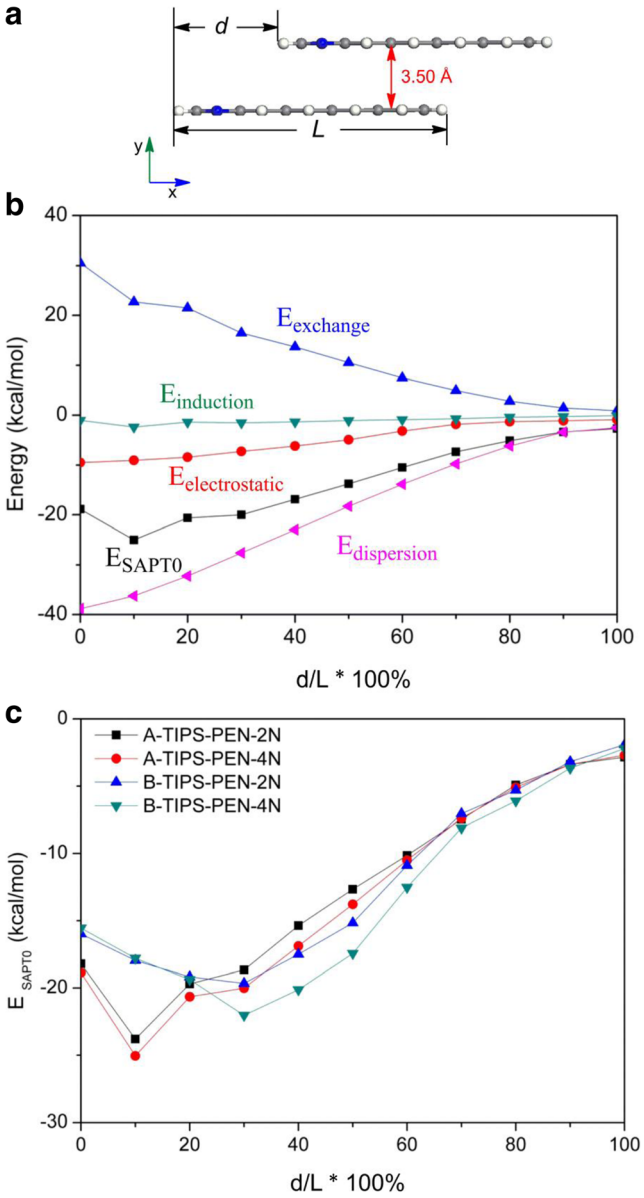


**Fig. 3** **a** Illustration of the structure of the dimer model used to calculate the intermolecular interactions. **b** Detailed components of the simplest energy from symmetry-adapted perturbation theory ($E_{SAPT0}$) for the series of *N*-heteropentacenes. **c** Comparison of $E_{SAPT0}$ for all of the molecules investigated in this study at different positions along the long axis

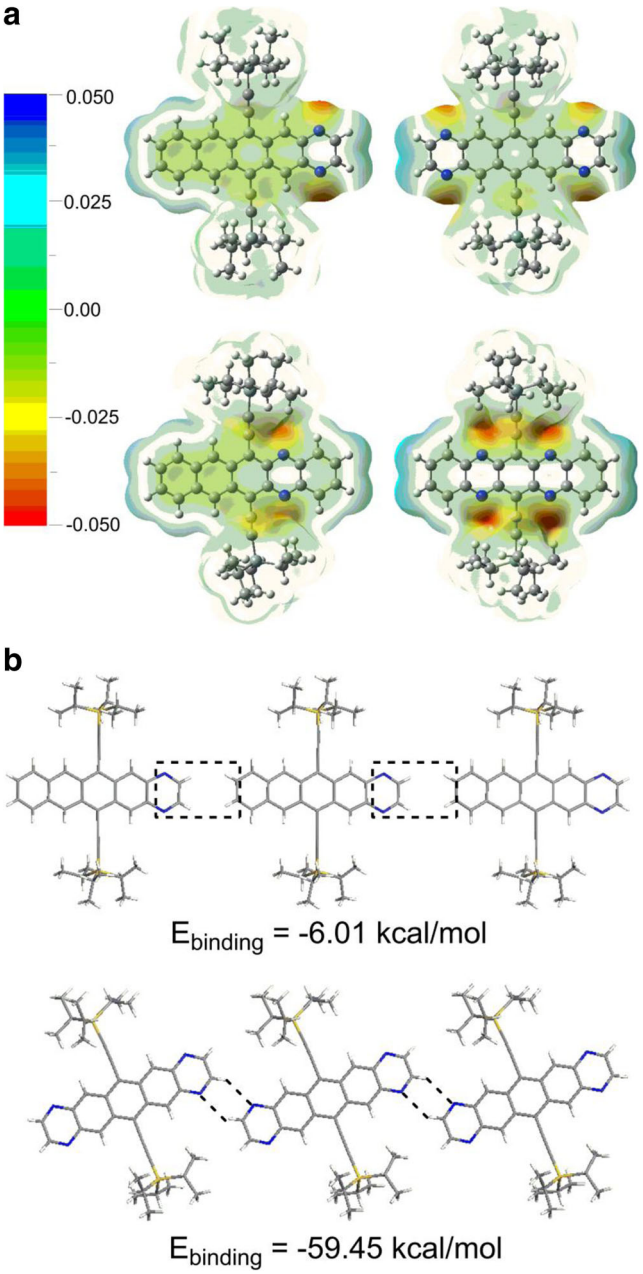


**Fig. 4** **a** Contour maps of electrostatic potential (in a.u.) for all molecules considered in this study, obtained using the DFT//B3LYP//6-31G (d,p) method. **b** Analysis of the binding energy in a single layer for the molecules A-TIPS-PEN-2N and A-TIPS-PEN-4N

the pyrazine rings because of the existence of lone-pair electrons. Strongly positive electrostatic potential areas are localized on the hydrogen atoms of the external rings. If electrostatic interactions are to occur between neighboring molecules, the relative positions of the molecules must be such that the distances between the nitrogen atoms of pyrazine rings in one molecule and the hydrogen atoms of the external rings in the other are short. However, from a molecular structure viewpoint, the large 3-D branches present in silylethynylated *N*-heteropentacenes can block electrostatic interactions with the internal three-ring core. Therefore, it appears that electrostatic interactions should only exist in molecules with external pyrazine rings, not molecules containing internal pyrazine rings. That is, only molecules A-TIPS-PEN-2N and A-TIPS-PEN-4N (which have external pyrazine rings) can change their molecular packing through electrostatic interactions. Upon carefully checking the molecular packing in one layer (see Fig. 4a), it was found that there are hardly any intermolecular hydrogen bonds for A-TIPS-PEN-2N due to the long distances between the dimers. On the other hand, for A-TIPS-PEN-4N, the C–H–N angles in the

double-pyrazine head-to-tail structures of neighboring dimers are 146°, and the distances are suitable for the formation of hydrogen bonds. The basis set superposition error (BSSE)-corrected binding energies of the dimers in systems containing external pyrazine rings were calculated with the M06-2X/6-31++G** method. The calculations yielded a binding energy of −6.01 kcal/mol$^{-1}$ for the A-TIPS-PEN-2N system, which is much smaller than that for the system A-TIPS-PEN-4N (−59.45 kcal/mol$^{-1}$). Thus, the different levels of electrostatic interaction present in these four *N*-heteropentacenes is thought to be the main reason for their different crystal structures.

The functional dependence of reorganization energy was examined and the results are shown in Fig. S1 of the "Electronic supplementary material," ESM. The corresponding hopping charge-transport factors (such as the distances between the centers of mass of the dimers and the transfer integrals for both holes and electrons) are gathered in Table 3. The values of $t_e$ are larger than those of $t_h$ for all dimers of the *N*-heteropentacenes considered here. To clarify the origin of this difference, the HOMO–HOMO/LUMO–LUMO coupling for pair 1 of A-TIPS-PEN-4N and B-TIPS-PEN-4N was investigated using the B3LYP/6-31G** method in the Multiwfn3.3.5 package [81, 82], and the overlap isosurface for the same isovalue is shown in Fig. 5. The regions covered by a positive isosurface (in red) and a negative isosurface (in blue) represent the overlap of orbital wavefunctions that are in the same phase and the overlap of those that are in opposite phases, respectively. For the LUMO–LUMO overlaps, negative isosurfaces are much smaller than positive isosurfaces. However, for HOMO–HOMO overlaps, the negative surfaces are nearly the same size as the positive regions. This clearly indicates that there is substantial cancellation between the positive and negative values in HOMO–HOMO overlaps but not in LUMO–LUMO overlaps. Consequently, the electron-transfer integrals (>100 meV) for dimers are much larger than the hole-transfer integrals (less than 10 meV). In addition, series A presents larger hole transfer integrals (6.34~44.06 meV) than series B ($t_h$ <5 meV). The transfer integrals in these *N*-heteropentacenes indicate that the introduction of external pyrazine rings may lead to bipolar materials, whereas we can be much more confident that the introduction of internal pyrazine rings will yield n-channel semiconductors.

Given the reorganization energies and transfer integrals, the hopping rate $k_i$ for each neighboring dimer can be obtained. The diffusion coefficient can then be calculated via kinetic Monte Carlo simulations. First, one random molecule in the supercell is chosen as the initial position and its nearest-neighboring molecules are assumed to be the next hopping points. Second, the hopping probability $p_{ij}$ is calculated as $k_{ij}/\sum k_{ij}$ and the hopping time as $1/k_{ij}$ for the nearest molecules $i$ and $j$. Third, a random number $r$ is generated which is uniformly distributed between 0 and 1. If $\sum p_{n-1} < r \leq \sum p_n$, the $n^{th}$ molecule is chosen as the hopping point. In each simulation, the displacement is recorded every 100 ns until the end of the simulation. This procedure is repeated thousands of times before a linear relationship between the mean-square displacement and the simulation time is obtained [62, 83]. Here, the total simulation time for each kinetic Monte Carlo simulation was set to 10,000 ns, and 2000 KMC simulations were performed to calculate the carrier mobility. The resulting linear relationship between mean-square displacement and simulation time is shown in Fig. 6.

The calculated carrier mobilities at 300 K are also listed in Table 3. These four *N*-heteropentacenes all possess large intrinsic electron mobilities in the range 0.84~3.58 cm$^2$ V$^{-1}$ s$^{-1}$. In addition, A-TIPS-PEN-2N and A-TIPS-PEN-4N exhibit p-channel behavior, with hole mobilities of 0.19 cm$^2$ V$^{-1}$ s$^{-1}$ and 0.09 cm$^2$ V$^{-1}$ s$^{-1}$, respectively. Although A-TIPS-PEN-4N presents large electron-transfer integrals, its calculated electron mobility (0.84 cm$^2$ V$^{-1}$ s$^{-1}$) is the smallest among the four *N*-heteropentacenes. As shown in Fig. 7a-b, the hopping pathways for A-TIPS-PEN-2N, B-TIPS-PEN-2N, and B-TIPS-PEN-4N are all similar to the typical 2-D π-stacking transport network. But the transport network for A-TIPS-PEN-4N shows sandwich-like π-stacking motifs, and the electron-transfer integrals between layers are much smaller than the transfer integrals in one layer (see Fig. S2 in the ESM). Thus, when checking the trajectories in our KMC simulations, it was found that electron-transport oscillations

**Table 3** Distances between the centers of mass of the dimers ($d_0$, in Å), DFT estimates of the transfer integrals of those dimers along the main transport pathways ($t$, in meV), simulated 2-D average mobilities ($\mu_{h\text{-}2D}/\mu_{e\text{-}2D}$, in cm$^2$ V$^{-1}$ s$^{-1}$) at 300 K, and corresponding experimental thin-film data ($\mu_{h\text{-}exp}/\mu_{e\text{-}exp}$, in cm$^2$ V$^{-1}$ s$^{-1}$) for holes and electrons, respectively

| | A-TIPS-PEN-2N | | A-TIPS-PEN-4N | | B-TIPS-PEN-2N | | B-TIPS-PEN-4N | |
|---|---|---|---|---|---|---|---|---|
| | p1 | p2 | p1 | p2 | p1 | p2 | p1 | p2 |
| $d_0$ | 7.95 | 9.93 | 7.64 | 8.55 | 7.72 | 10.01 | 7.61 | 9.96 |
| $t_h$ | 7.81 | 17.09 | 6.34 | 44.06 | 4.08 | 2.80 | 2.38 | 0.31 |
| $t_e$ | 97.14 | 77.15 | 109.00 | 19.63 | 101.34 | 50.00 | 102.65 | 42.30 |
| $\mu_{h\text{-}2D}$ | 0.19 | | 0.09 | | 0.01 | | $6.97\times10^{-4}$ | |
| $\mu_{h\text{-}exp}$ | 0.3–1.2[29] | | 0.05–0.22[29] | | 0.02–0.05[30] | | - | |
| $\mu_{e\text{-}2D}$ | 3.58 | | 0.84 | | 2.31 | | 2.04 | |
| $\mu_{e\text{-}exp}$ | - | | 0.3–1.1[29] | | 0.0002–0.0004[30] | | 0.3–0.5, 1.0–3.3[30] | |

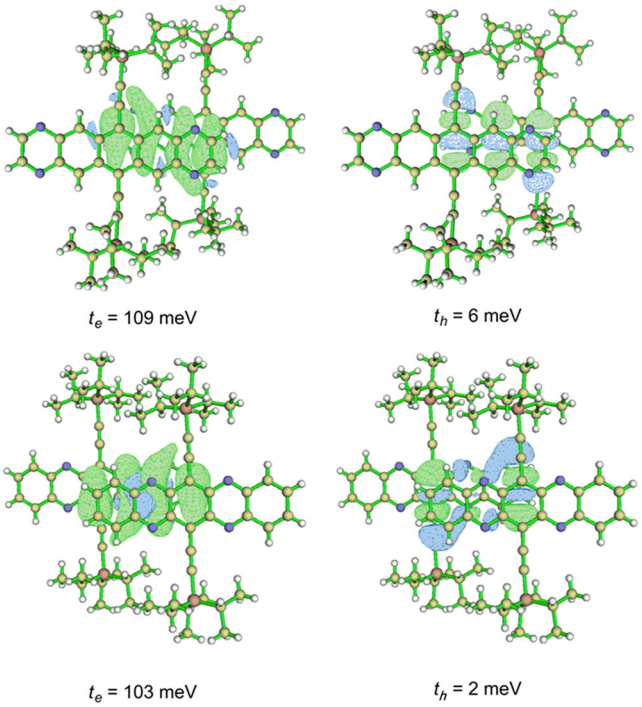


**Fig. 5** Molecular orbital overlap for pair 1 of A-TIPS-PEN-4N and B-TIPS-PEN-4N

occur, leading to long latent times between hops from dimer to dimer in a layer. These oscillations hinder the charge-hopping process between layers and hence limit the electron mobility. This also indicates that besides the traditional main hopping-transport factors, such as the reorganization energies and transfer integrals, charge-transport networks should be considered when designing organic semiconductor materials.

From the carrier mobility results shown in Table 3, it is clear that the calculated electron mobilities of A-TIPS-PEN-4N and B-TIPS-PEN-4N are consistent with the corresponding experimental values. However, the predicted electron

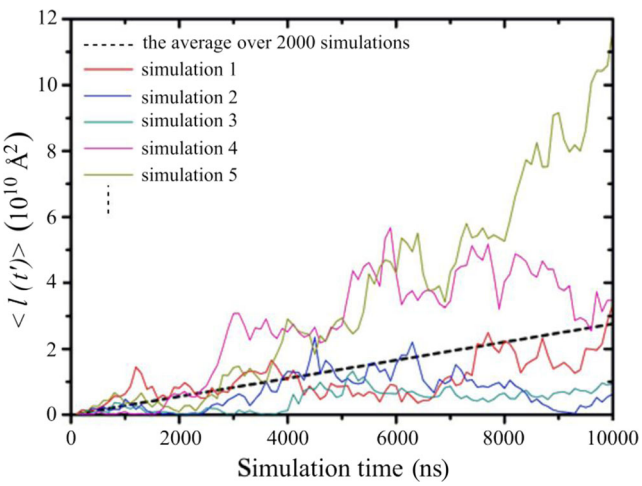


**Fig. 6** Plots of mean-square displacement versus simulation time for typical KMC simulations, and the average linear relationship between mean-square displacement and simulation time for 2000 simulations

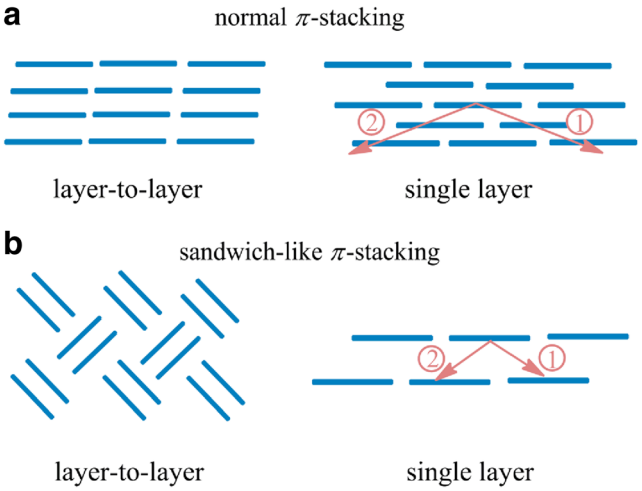


**Fig. 7a–b** Molecular packing and charge-transport networks for the series of *N*-heteropentacenes: **a** normal π-stacking for A-TIPS-PEN-2N, B-TIPS-PEN-2N, and B-TIPS-PEN-4N; **b** sandwich-like π-stacking for A-TIPS-PEN-4N

mobilities of A-TIPS-PEN-2N and B-TIPS-PEN-2N are considerably higher than the actual values. It should be noted that the trend in the predicted average electron mobilities for series B agrees well with that seen in recently reported theoretical results [84]. That is, the average 2-D electron mobilities of B-TIPS-PEN-2N and B-TIPS-PEN-4N are of the same order of magnitude, with the former being slightly larger than the latter. The high electron injection energy barriers (assuming the use of gold electrodes) at the metal–organic semiconductor interface and the poor molecular stability of molecules with just one pyrazine ring may lead to the difference between the theoretical results and the experimental mobilities. Also, the simulated carrier mobility values are based on ideal single-crystal devices, which are much more ordered and contain fewer defects than the thin-film OFETs used in experiments.

Although the hopping mechanism has been used to describe the charge transport behavior in these *N*-heteropentacene materials, it is important to mention that the semiclassical Marcus electron transfer theory cannot help us to elucidate all aspects of the charge-transport process. A recent study has also demonstrated the simultaneous presence of band carriers and incoherent states in crystalline organic semiconductors with band-like transport behavior, and that the respective contribution to carrier mobility is dependent on the temperature [85]. The relevant transport parameters in the band-like mechanism should therefore also be discussed in order to achieve a relatively comprehensive understanding of their charge-transport properties.

## Band structure and effective mass

In the standard band-theory model, the charge moves coherently in a wavelike manner, and the electronic band structures can reflect the anisotropic carrier transport properties of the

solid-state materials. In this case, the carrier mobility for the band-like mechanism can be expressed as follows:

$$\mu = \frac{q\tau}{m}, \tag{8}$$

where $q$ denotes the charge of the carrier, $\tau$ is the mean relaxation time of the band state, and $m$ is the effective mass [86]. In general, the valence/conduction band (VB/CB) consists of sub-bands arising from interactions among the monomer HOMO/LUMO levels. Notably, the number of sub-bands is equal to the number of molecules in the primitive unit cell for nondegenerate monomer energy levels [54].

The calculated band structures of the *N*-heteropentacenes included in this study are shown in Fig. 8. For the systems A-TIPS-PEN-2N, B-TIPS-PEN-2N, and B-TIPS-PEN-4N, there is a single sub-band in the conduction band and in the valence band since there is only one molecule in the unit cell. However, there are four molecules in the unit cell of the A-TIPS-PEN-4N crystal, and half of them are geometrically equivalent, with specific mirror symmetry. The result is two by two quasi-degenerate sub-bands. The molecular crystals A-TIPS-PEN-2N, B-TIPS-PEN-2N, and B-TIPS-PEN-4N have similar crystal packing structures, so the shapes of their CBs and VBs are also very similar, and strong orientation anisotropy of the band dispersion is observed. Importantly, they present large bandwidths of their CBs (548~663 meV), which are comparable to those computed for the pentacene crystal (590 meV for CB) [87] and for substituted PTCDI molecules (649 meV for CB) [54]. These results are consistent with those from transfer integral calculations, where significant electronic couplings are only found for the π-stacking dimers. It also indicates that these molecules are probably promising candidates for n-type materials. Their valence bands are relatively flat, with small bandwidths (36~113 meV). Greater band dispersion would lead to a smaller effective mass and hence higher band-like carrier mobility.

To further understand their charge-transport properties in the framework of band-like transport theory, the effective masses were calculated and are listed in Table 4. As a consequence of large CB dispersions, the effective electron masses along the π-stacking direction are very small (0.641 $m_0$, 0.852 $m_0$, 0.731 $m_0$, and 0.847 $m_0$ respectively; here, $m_0$ represents the rest mass of a free electron), which should be highly beneficial to electron transport. Interestingly, although

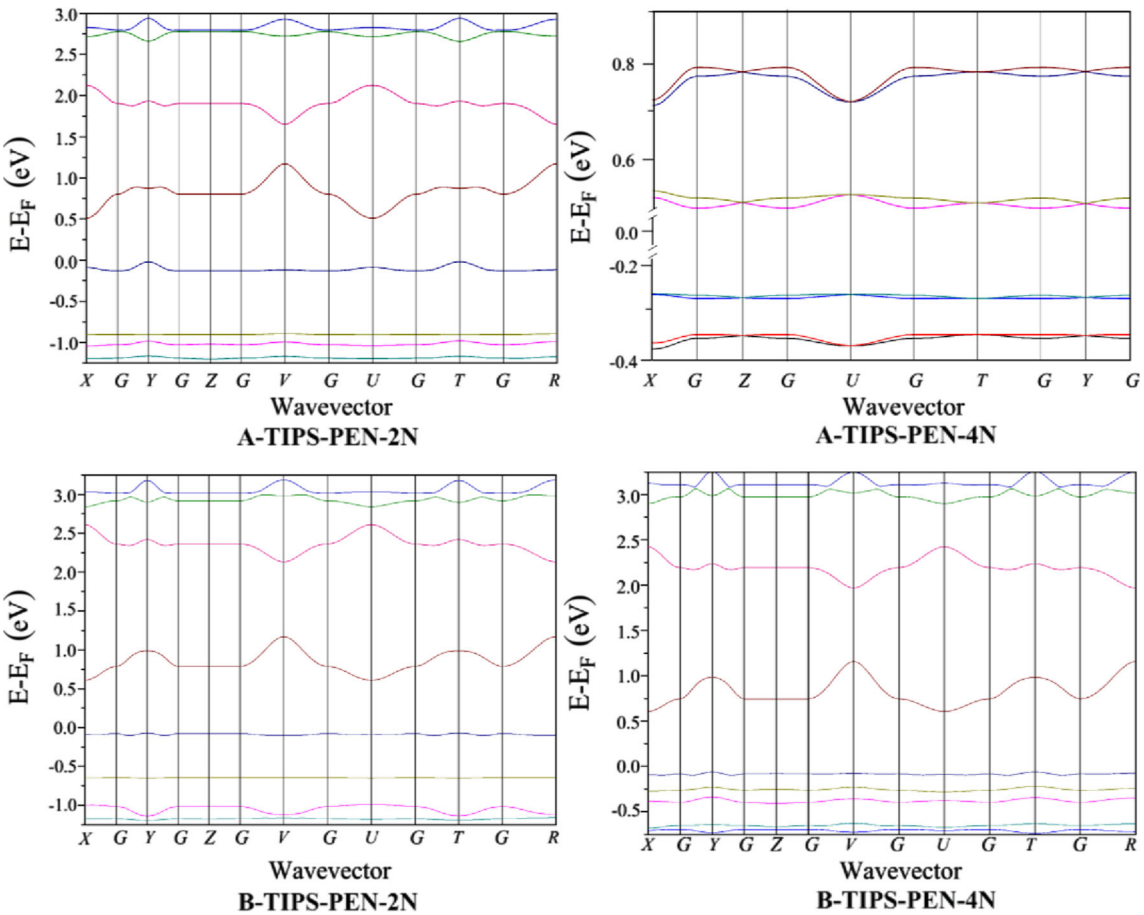


**Fig. 8** Illustration of the energy band structures for the molecular crystals investigated in this study. The points of high symmetry in the first Brillouin zone are labeled as follows: G=(0, 0, 0); X=(0.5, 0, 0); Y=(0, 0.5, 0); Z=(0, 0, 0.5); V=(0.5, 0.5, 0); U=(0.5, 0, 0.5); T=(0, 0.5, 0.5); R=(0.5, 0.5, 0.5), all in crystallographic coordinates. The zero point in energy is taken to be the Fermi energy level

**Table 4** Principal components of the effective hole and electron masses $m$ (in units of the rest mass of a free electron $m_0$)

| Compound | Hole | | Electron | |
|---|---|---|---|---|
| | $m_1$ | $m_2$ | $m_1$ | $m_2$ |
| A-TIPS-PEN-2N | 5.103 | 1.060 | 0.641 | 1.370 |
| A-TIPS-PEN-4N | 6.082 | 2.428 | 0.852 | 2.111 |
| B-TIPS-PEN-2N | 2.329 | 12.458 | 0.731 | 1.701 |
| B-TIPS-PEN-4N | 2.716 | 13.305 | 0.847 | 2.072 |

the electron transfer integral values in our systems and for pentacene are comparable, the effective masses are much smaller in the former (in pentacene, the smallest effective electron mass component is about 1.7 $m_0$ [88, 89]). This result can be explained by the fact that the effective mass at the band edge also depends on the effective hopping distance ($m=\hbar^2/2td^2$, where $d$ is distance) in the one-dimensional tight-binding model. This distance along the stacking direction in these systems is much larger than the characteristic distances between the nearest-neighbor molecules in pentacene with herringbone molecular stacking. In addition, the systems A-TIPS-PEN-2N and B-TIPS-PEN-2N (with only one pyrazine ring) possess smaller effective masses than the systems A-TIPS-PEN-4N and A-TIPS-PEN-4N (with two pyrazine rings). This tendency is also consistent with the results for the hopping mechanism.

In fact, molecules are held together by weak interactions in organic semiconductors, and the electron coupling between adjacent molecules is rather sensitive to geometric parameters [56]. The fluctuations in the electronic coupling caused by thermal molecular motions can be of the same order of magnitude as the static value [90]. Thus, we also considered the role of dynamic disorder in the charge-transport properties of *N*-heteropentacenes.

## Dynamic disorder

The combined molecular dynamics (MD) and quantum-chemical calculation approach was employed to estimate the thermodynamic vibrations of the transfer integrals. The MD simulations were carried out in the Discover module of the Materials Studio package using the COMPASS force field [91]. To avoid potential artificial symmetry effects, 5×5×5 supercells were built based on their crystal structures. Each system was equilibrated using the Andersen thermostat with the NVT ensemble at 300 K, and the simulation time step was set to 1 fs. After thermal equilibration for 200 ps, one frame was extracted every 100 fs until the total simulation time reached 100 ps (see Fig. 9).

The vibration of the lattice has a dual effect on the charge transport process. On the one hand, nonlocal electron–phonon coupling leads to a phonon-assisted contribution to the hopping mobility due to the variation ($\sigma$) in the transfer integral: $\langle t^2\rangle=\langle t_0\rangle^2+\sigma^2$. Here, the effect of nonlocal electron–phonon coupling on hopping carrier mobility is defined as the ratio $t^2/t_0^2$. From Table 5, the differences between $t^2$ and $t_0^2$ are only 0.02~0.08, and the values of $t^2/t_0^2$ are all similar to each other, which demonstrates that the lattice vibrations have little influence on the hopping carrier mobilities. This phenomenon can be attributed to balanced thermal fluctuations of the nearest-neighboring dimers in the same direction, similar to the pentacene case. On the other hand, the lattice vibrations also decrease the band-like carrier mobility through a scattering mechanism. The relaxation time is given by $\frac{\hbar}{\tau}\propto\frac{L}{t_0}k_BT$ [85, 92]. Therefore, a larger $L/t_0$ means a shorter relaxation time, which will increase the band carrier mobility. Here, $L$ has a similar physical meaning to $\lambda$, which indicates the overall strength of nonlocal electron–phonon coupling. The lattice relaxation energy $L$ can be calculated from the variation ($\sigma$) in the transfer integral at the high-temperature limit: $\sigma^2=\langle t^2\rangle-\langle t_0\rangle^2=2LK_BT$ [86]. As shown in Table 5, the values of $L/t_0$ in

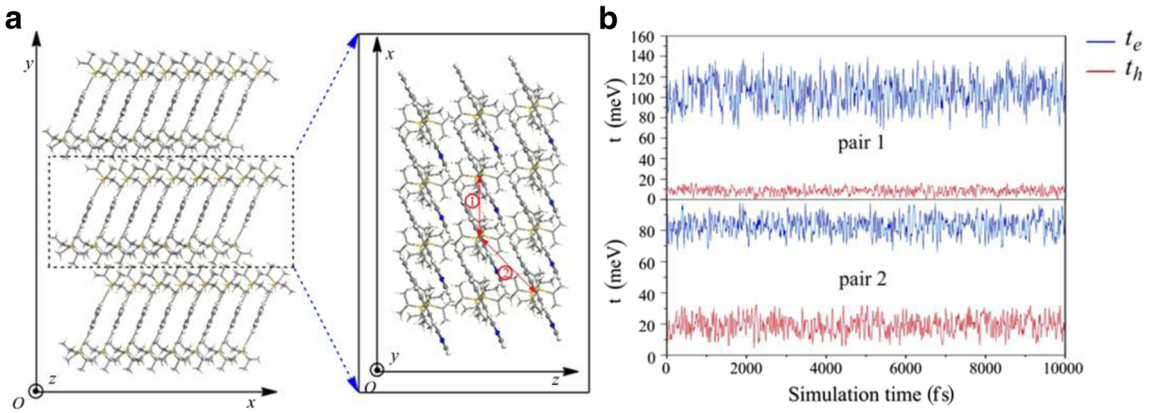


**Fig. 9** **a** Sketch of the supercell model (based on the crystal structure of A-TIPS-PEN-2N) that was used to investigate dynamic disorder, and a single layer extracted from the supercell. Here, $x$, $y$, and $z$ are the reference axes. **b** Thermal fluctuations during simulations of the hole and electron transfer integrals for pair 1 and pair 2 at 300 K

**Table 5** Molecular dynamics estimates of $\sigma$, $L$, $t^2/t_0^2$, and $L/t_0$ for the main dimers in the studied *N*-heteropentacenes

| | A-TIPS-PEN-2N | | A-TIPS-PEN-4N | |
|---|---|---|---|---|
| | p1 | p2 | p1 | p2 |
| $\sigma$ (meV) | 35.19 | 15.03 | 29.56 | 15.83 |
| $L$ (meV) | 23.95 | 4.37 | 16.90 | 4.85 |
| $t^2/t_0^2$ | 1.06 | 1.02 | 1.04 | 1.03 |
| $L/t_0$ | 0.25 | 0.06 | 0.15 | 0.25 |
| | B-TIPS-PEN-2N | | B-TIPS-PEN-4N | |
| | p1 | p2 | p1 | p2 |
| $\sigma$ (meV) | 32.16 | 20.38 | 26.69 | 17.66 |
| $L$ (meV) | 20.01 | 8.03 | 13.78 | 6.03 |
| $t^2/t_0^2$ | 1.05 | 1.08 | 1.03 | 1.08 |
| $L/t_0$ | 0.20 | 0.16 | 0.13 | 0.14 |

pair 1 for systems with one pyrazine are a bit larger than those for systems with two pyrazines. This demonstrates that the scattering process along the main charge-transfer direction in molecules with one pyrazine is stronger than that in molecules with two pyrazine rings. It is interesting to note that values of $L/t_0$ can vary for the same system. For example, $L/t_0$ of pair 1 in A-TIPS-PEN-2N is 0.25, which is much larger than that of pair 2 ($L/t_0$=0.06). This implies that the scattering process may be anisotropic for different molecular dimers.

The effect of dynamic disorder on the anisotropic mobilities and the ultimate intrinsic electron mobilities of these systems were also investigated. Here, we use the *ab* planes of the systems A-TIPS-PEN-2N, B-TIPS-PEN-2N, and B-TIPS-PEN-4N as examples. The following equation was adopted to calculate the anisotropic mobilities [93, 94]:

$$\mu_{\text{anisotropic}} = \frac{e}{2K_{\text{B}}T} \lim_{t'\to\infty} \sum \frac{x(t')^2 \cos^2\gamma_i \cos^2(\phi_i - \Phi)}{t'}, \qquad (9)$$

where $\gamma_i$ and $\phi_i$ are angles in relation to the reference axis. The crystallographic *b* axis was set as the reference axis, and all $\gamma_i$ should be zero for 2-D charge transport in the *ab* plane. The results for the simulated 2-D anisotropic electron mobilities with and without dynamic disorder are displayed in detail in Fig. 10. Due to the rather small differences between $t_0$ and $t$, the electron mobilities in the same direction are very similar with or without dynamic disorder. It can also be seen that the electron mobilities for these *N*-heteropentacenes in the *ab* plane show remarkably anisotropic transport behavior. For A-TIPS-BEN-2N, the highest electron mobility values are 5.56 $cm^2\ V^{-1}\ s^{-1}$ without dynamic disorder and 5.81 $cm^2\ V^{-1}\ s^{-1}$ in the disorder case, where $\Phi$ =160°/340°. The enhanced electron mobility in the latter case can be explained by phonon-assisted transport behavior, where nonlocal coupling contributions are introduced into the squared transfer integrals: $\langle t^2\rangle = \langle t_0\rangle^2 + \sigma^2$. According to Eq. 1, the average hopping rate should increase, as it is proportional to $<t^2>$. Since the transfer integrals for pairs 1 and 2 are of the same magnitude, the anisotropic electron mobilities should be greatly influenced by these two pathways according to Eq. 9. For systems with internal pyrazine rings, the highest electron mobilities occur in the direction with the maximal transfer integrals, where $\Phi$ =0°/180°, because the main contribution to anisotropic mobility derives from the electron mobility along the *b* axis. For B-TIPS-PEN-2N and B-TIPS-PEN-4N, the highest electron mobilities with dynamic disorder are 5.77 $cm^2\ V^{-1}\ s^{-1}$ and 6.59 $cm^2\ V^{-1}\ s^{-1}$, respectively. Considering that the range of electron mobilities for B-TIPS-PEN-4N is wider than that for B-TIPS-PEN-2N, it is reasonable that the average electron mobility of the former is slightly smaller than that of the latter.

Using the results of the systematic theoretical investigation reported above, we now attempt to answer the questions posed in the "Introduction." Although A-TIPS-PEN-2N possesses comparable intrinsic electron mobility to the highest values seen for these *N*-heteropentacenes, its poor stability and high injection energy barrier would be expected to limit its performance in experimental measurements. Although A-TIPS-PEN-4N is more stable, it suffers from poor charge-transport networks in sandwich π-stacking motifs and thus low electron mobility. B-TIPS-PEN-2N and B-TIPS-PEN-4N, with internal pyrazine rings, have been calculated to have intrinsic electron mobilities of the same order of magnitude, which is inconsistent with experimental results. Further, the highest electron mobility of B-TIPS-PEN-4N (6.59 $cm^2\ V^{-1}\ s^{-1}$) is larger than that of B-TIPS-PEN-2N (5.77 $cm^2\ V^{-1}\ s^{-1}$). At present, it appears that introducing two internal pyrazine rings into TIPS-PEN offers the best combination of high electron mobility and good stability, in contrast with the results seen for TA-PEN. It is also useful to recall that real device performance is dictated by these two mechanisms as well as other practical factors, such as the charge-transport process at the metal–organic semiconductor interface, the effect of impurities on charge-transport properties, and so on [95]. However, such a comprehensive investigation would require a substantial upgrade in the theoretical model used, which is beyond the scope of the present work.

## Conclusion

To summarize, we have theoretically investigated the effect of the number of pyrazines and their positions on the charge-transport properties of four silylethynylated *N*-heteropentacenes, considering both the hopping and band-like mechanisms. Fluctuations in their transfer integrals were also studied via the mixed quantum chemistry and molecular dynamics approach. The results show that systems with

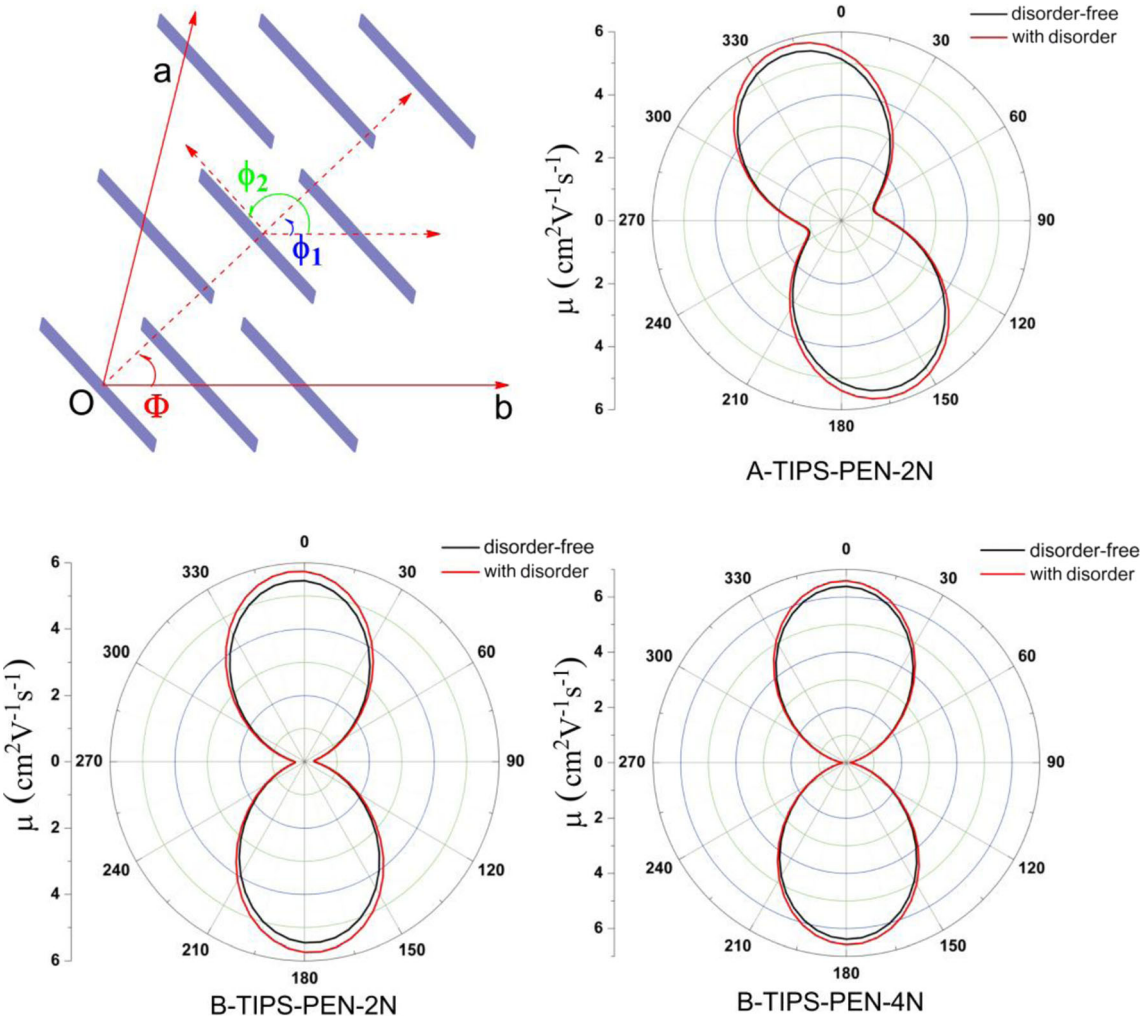


**Fig. 10** 2-D anisotropic electron mobilities in the *ab* planes of A-TIPS-PEN-2N, B-TIPS-PEN-2N, and B-TIPS-PEN-4N, with and without dynamic disorder. Here, *a* and *b* refer to the crystal axes

internal pyrazine rings possess relatively low electron injection barriers and better stability in the ambient atmosphere. The mobilities calculated for the hopping mechanism suggest that molecules with external pyrazine rings are bipolar materials while molecules containing internal pyrazine rings tend to be n-type materials. The limited electron mobility of A-TIPS-PEN-4N indicates that, besides the traditional main hopping transport factors such as the reorganization energies and transfer integrals, the charge-transport network should be also taken into consideration when designing new materials. The electronic band structures of the *N*-heteropentacenes and the effective masses of the band-like mechanism were also studied. The results obtained for band-like charge transport indicate that these four *N*-heteropentacenes should be good n-type organic semiconductors. It was also found that fluctuations in transfer integrals have little effect on the hopping carrier mobilities of these *N*-heteropentacenes. Our theretical results demonstrate that it is more advantageous to introduce internal than external pyrazine moieties in terms of enhancing air stability and charge-transport networks. Although the electron mobility of B-TIPS-PEN-4N was found experimentally to be four orders of magnitude larger than that of B-TIPS-PEN-2N, our theoretical investigation clearly indicates that the experimental results are not an accurate reflection of the intrinsic charge-transport properties of these molecules. The highest intrinsic electron mobilities of B-TIPS-PEN-2N and B-TIPS-PEN-4N are 5.77 $cm^2\ V^{-1}\ s^{-1}$ and 6.59 $cm^2\ V^{-1}\ s^{-1}$, respectively, which demonstrates that there is still room to improve the performance of each in experiments based on single-crystal devices rather than films. Among the four silylethynylated *N*-heteropentacenes investigated, our results suggest that B-TIPS-PEN-4N is the most promising n-type material from the combined perspectives of electron mobility and air stability.

**Acknowledgments** Dr. Hui Li (Jilin University) is acknowledged for providing instructions on the program VASP. This work was supported by the Natural Science Foundation of China (nos. 20973078 and 21173099),

the Major State Basis Research Development Program (2013CB834801), Special Funding to Basic Scientific Research Projects for Central Colleges, as well as the Graduate Innovation Fund of Jilin University (no. 20121029).

## References


1. Tang CW, VanSlyke SA (1987) Organic electroluminescent diodes. Appl Phys Lett 51(12):913. doi:10.1063/1.98799
2. Ho PK, Kim JS, Burroughes JH, Becker H, Li SF, Brown TM, Cacialli F, Friend RH (2000) Molecular-scale interface engineering for polymer light-emitting diodes. Nature 404(6777):481–484. doi:10.1038/35006610
3. Katz HE (1997) Organic molecular solids as thin film transistor semiconductors. J Mater Chem 7(3):369–376. doi:10.1039/a605274f
4. Horowitz G, Hajlaoui ME (2000) Mobility in polycrystalline oligothiophene field-effect transistors dependent on grain size. Adv Mater 12(14):1046–1050. doi:10.1002/1521-4095(200007)12:14<1046::Aid-Adma1046>3.3.Co;2-N
5. Newman CR, Frisbie CD, da Silva DA, Bredas JL, Ewbank PC, Mann KR (2004) Introduction to organic thin film transistors and design of n-channel organic semiconductors. Chem Mater 16(23):4436–4451. doi:10.1021/cm049391x
6. Padinger F, Rittberger RS, Sariciftci NS (2003) Effects of postproduction treatment on plastic solar cells. Adv Funct Mater 13(1):85–88. doi:10.1002/adfm.200390011
7. Brabec CJ, Sariciftci NS, Hummelen JC (2001) Plastic solar cells. Adv Funct Mater 11(1):15–26. doi:10.1002/1616-3028(200102)11:1<15::aid-adfm15>3.3.co;2-1
8. Li L, Gao P, Baumgarten M, Mullen K, Lu N, Fuchs H, Chi L (2013) High performance field-effect ammonia sensors based on a structured ultrathin organic semiconductor film. Adv Mater 25(25):3419–3425. doi:10.1002/adma.201301138
9. Shaymurat T, Tang Q, Tong Y, Dong L, Liu Y (2013) Gas dielectric transistor of CuPc single crystalline nanowire for SO(2) detection down to sub-ppm levels at room temperature. Adv Mater 25(16):2269–2273. doi:10.1002/adma.201204509, 2376
10. Someya T, Kato Y, Sekitani T, Iba S, Noguchi Y, Murase Y, Kawaguchi H, Sakurai T (2005) Conformable, flexible, large-area networks of pressure and thermal sensors with organic transistor active matrixes. Proc Natl Acad Sci USA 102(35):12321–12325. doi:10.1073/pnas.0502392102
11. Torsi L, Magliulo M, Manoli K, Palazzo G (2013) Organic field-effect transistor sensors: a tutorial review. Chem Soc Rev 42(22):8612–8628. doi:10.1039/c3cs60127g
12. Sundar VC, Zaumseil J, Podzorov V, Menard E, Willett RL, Someya T, Gershenson ME, Rogers JA (2004) Elastomeric transistor stamps: reversible probing of charge transport in organic crystals. Science 303(5664):1644–1646. doi:10.1126/science.1094196
13. De Longchamp DM, Kline RJ, Lin EK, Fischer DA, Richter LJ, Lucas LA, Heeney M, McCulloch I, Northrup JE (2007) High carrier mobility polythiophene thin films: structure determination by experiment and theory. Adv Mater 19(6):833. doi:10.1002/adma.200602651
14. Zhang M, Tsao HN, Pisula W, Yang C, Mishra AK, Mullen K (2007) Field-effect transistors based on a benzothiadiazole-cyclopentadithiophene copolymer. J Am Chem Soc 129(12):3472–3473. doi:10.1021/ja0683537
15. Huang C, West JE, Katz HE (2007) Organic field-effect transistors and unipolar logic gates on charged electrets from spin-on organosilsesquioxane resins. Adv Funct Mater 17(1):142–153. doi:10.1002/adfm.200600690
16. Anthony JE (2006) Functionalized acenes and heteroacenes for organic electronics. Chem Rev 106(12):5028–5048. doi:10.1021/cr050966z
17. Kastler M, Laquai F, Mullen K, Wegner G (2006) Room-temperature nondispersive hole transport in a discotic liquid crystal. Appl Phys Lett 89(25):252103. doi:10.1063/1.2408654
18. Naraso NJ, Kumaki D, Tokito S, Yamashita Y (2006) High performance n- and p-type field-effect transistors based on tetrathiafulvalene derivatives. J Am Chem Soc 128(30):9598–9599. doi:10.1021/ja0630083
19. Chabinyc ML, Salleo A, Wu Y, Liu P, Ong BS, Heeney M, McCulloch I (2004) Lamination method for the study of interfaces in polymeric thin film transistors. J Am Chem Soc 126(43):13928–13929. doi:10.1021/ja044884o
20. Takimiya K, Shinamura S, Osaka I, Miyazaki E (2011) Thienoacene-based organic semiconductors. Adv Mater 23(38):4347–4370. doi:10.1002/adma.201102007
21. Menard E, Podzorov V, Hur SH, Gaur A, Gershenson ME, Rogers JA (2004) High-performance n- and p-type single-crystal organic transistors with free-space gate dielectrics. Adv Mater 16(23–24):2097–2012. doi:10.1002/adma.200401017
22. Podzorov V, Menard E, Rogers JA, Gershenson ME (2005) Hall effect in the accumulation layers on the surface of organic semiconductors. Phys Rev Lett 95(22):226601. doi:10.1103/PhysRevLett.95.226601
23. Zaumseil J, Sirringhaus H (2007) Electron and ambipolar transport in organic field-effect transistors. Chem Rev 107(4):1296–1323. doi:10.1021/cr0501543
24. Crone B, Dodabalapur A, Lin YY, Filas RW, Bao Z, LaDuca A, Sarpeshkar R, Katz HE, Li W (2000) Large-scale complementary integrated circuits based on organic transistors. Nature 403(6769):521–523. doi:10.1038/35000530
25. Nishida J, Naraso N, Murai S, Fujiwara E, Tada H, Tomura M, Yamashita Y (2004) Preparation, characterization, and FET properties of novel dicyanopyrazinoquinoxaline derivatives. Org Lett 6(12):2007–2010. doi:10.1021/ol0494010
26. Nakagawa T, Kumaki D, Nishida JI, Tokito S, Yamashita Y (2008) High performance n-type field-effect transistors based on indenofluorenedione and diindenopyrazinedione derivatives. Chem Mater 20(8):2615–2617. doi:10.1021/Cm800366b
27. Wang H, Wen Y, Yang X, Wang Y, Zhou W, Zhang S, Zhan X, Liu Y, Shuai Z, Zhu D (2009) Fused-ring pyrazine derivatives for n-type field-effect transistors. ACS Appl Mater Interfaces 1(5):1122–1129. doi:10.1021/am900093p
28. Tang Q, Zhang DQ, Wang SL, Ke N, Xu JB, Yu JC, Miao Q (2009) A meaningful analogue of pentacene: charge transport, polymorphs, and electronic structures of dihydrodiazapentacene. Chem Mater 21(7):1400–1405. doi:10.1021/Cm9001916
29. Liang Z, Tang Q, Mao R, Liu D, Xu J, Miao Q (2011) The position of nitrogen in N-heteropentacenes matters. Adv Mater 23(46):5514–5518. doi:10.1002/adma.201103759
30. Liang Z, Tang Q, Xu J, Miao Q (2011) Soluble and stable N-heteropentacenes with high field-effect mobility. Adv Mater 23(13):1535–1539. doi:10.1002/adma.201004325
31. Chen HY, Chao I (2006) Toward the rational design of functionalized pentacenes: reduction of the impact of functionalization on the reorganization energy. Chemphyschem 7(9):2003–2007. doi:10.1002/cphc.200600266
32. Winkler M, Houk KN (2007) Nitrogen-rich oligoacenes: candidates for n-channel organic semiconductors. J Am Chem Soc 129(6):1805–1815. doi:10.1021/ja067087u
33. Chen XK, Guo JF, Zou LY, Ren AM, Fan JX (2011) A promising approach to obtain excellent n-type organic field-effect transistors: introducing pyrazine ring. J Phys Chem C 115(43):21416–21428. doi:10.1021/Jp206617e
34. Tang Q, Liang Z, Liu J, Xu J, Miao Q (2010) N-heteroquinones: quadruple weak hydrogen bonds and n-channel transistors. Chem Commun (Camb) 46(17):2977–2979. doi:10.1039/c001215g
35. Liang Z, Tang Q, Liu J, Li J, Yan F, Miao Q (2010) N-type organic semiconductors based on π-deficient pentacenequinones: synthesis,

electronic structures, molecular packing, and thin film transistors. Chem Mater 22(23):6438–6443. doi:10.1021/cm102681p
36. Zhang W, Zhong X, Zhao Y (2012) Electron mobilities of n-type organic semiconductors from time-dependent wavepacket diffusion method: pentacenequinone derivatives. J Phys Chem A 116(46): 11075–11082. doi:10.1021/jp3023474
37. Miao Q (2012) N-heteropentacenes and N-heteropentacenequinones: from molecules to semiconductors. Synlett 23(3):326–336. doi:10.1055/s-0031-1290323
38. Anthony JE, Eaton DL, Parkin SR (2002) A road map to stable, soluble, easily crystallized pentacene derivatives. Org Lett 4(1):15–18. doi:10.1021/ol0167356
39. Bässler H (1993) Charge transport in disordered organic photoconductors a Monte Carlo simulation study. Phys Status Solidi B 175(1):15–56. doi:10.1002/pssb.2221750102
40. Vissenberg MCJM, Matters M (1998) Theory of the field-effect mobility in amorphous organic transistors. Phys Rev B 57(20): 12964–12967. doi:10.1103/PhysRevB.57.12964
41. Meijer EJ, Tanase C, Blom PWM, van Veenendaal E, Huisman BH, de Leeuw DM, Klapwijk TM (2002) Switch-on voltage in disordered organic field-effect transistors. Appl Phys Lett 80(20):3838–3840. doi:10.1063/1.1479210
42. Tanase C, Meijer EJ, Blom PWM, de Leeuw DM (2003) Local charge carrier mobility in disordered organic field-effect transistors. Org Electron 4(1):33–37. doi:10.1016/S1566-1199(03)00006-5
43. Tanase C, Meijer EJ, Blom PW, De Leeuw DM (2003) Unification of the hole transport in polymeric field-effect transistors and light-emitting diodes. Phys Rev Lett 91(21):216601. doi:10.1103/PhysRevLett.91.216601
44. Warta W, Stehle R, Karl N (1985) Ultrapure, high mobility organic photoconductors. Appl Phys A 36(3):163–170. doi:10.1007/BF00624938
45. Ostroverkhova O, Cooke DG, Shcherbyna S, Egerton RF, Hegmann FA, Tykwinski RR, Anthony JE (2005) Bandlike transport in pentacene and functionalized pentacene thin films revealed by subpicosecond transient photoconductivity measurements. Phys Rev B 71(3):035204. doi:10.1103/Physrevb.71.035204
46. Ostroverkhova O, Cooke DG, Hegmann FA, Anthony JE, Podzorov V, Gershenson ME, Jurchescu OD, Palstra TTM (2006) Ultrafast carrier dynamics in pentacene, functionalized pentacene, tetracene, and rubrene single crystals. Appl Phys Lett 88(16):162101. doi:10.1063/1.2193801
47. Podzorov V, Menard E, Borissov A, Kiryukhin V, Rogers JA, Gershenson ME (2004) Intrinsic charge transport on the surface of organic semiconductors. Phys Rev Lett 93(8):086602. doi:10.1103/PhysRevLett.93.086602
48. Marcus RA (1993) Electron transfer reactions in chemistry. Theory and experiment. Rev Mod Phys 65(3):599–610. doi:10.1103/RevModPhys.65.599
49. Becke AD (1988) Density-functional exchange-energy approximation with correct asymptotic behavior. Phys Rev A 38(6):3098–3100. doi:10.1103/PhysRevA.38.3098
50. Lee C, Yang W, Parr RG (1988) Development of the Colle–Salvetti correlation-energy formula into a functional of the electron density. Phys Rev B 37(2):785–789. doi:10.1103/PhysRevB.37.785
51. Stephens PJ, Devlin FJ, Chabalowski CF, Frisch MJ (1994) Ab initio calculation of vibrational absorption and circular dichroism spectra using density functional force fields. J Phys Chem 98(45):11623–11627. doi:10.1021/j100096a001
52. Geng Y, Wang J, Wu S, Li H, Yu F, Yang G, Gao H, Su Z (2011) Theoretical discussions on electron transport properties of perylene bisimide derivatives with different molecular packings and intermolecular interactions. J Mater Chem 21(1):134–143. doi:10.1039/c0jm02119a
53. Li C-H, Huang C-H, Kuo M-Y (2011) Halogenated 6,13-bis(triisopropylsilylethynyl)-5,7,12,14-tetraazapentacene: applications for ambipolar air-stable organic field-effect transistors. Phys Chem Chem Phys 13(23):11148–11155. doi:10.1039/c1cp20391f
54. Delgado MCR, Kim E-G, da Silva Filho DA, Bredas J-L (2010) Tuning the charge-transport parameters of perylene diimide single crystals via end and/or core functionalization: a density functional theory investigation. J Am Chem Soc 132(10):3375–3387. doi:10.1021/ja908173x
55. Frisch MJ, Trucks GW, Schlegel HB, Scuseria GE, Robb MA, Cheeseman JR, Scalmani G, Barone V, Mennucci B, Petersson GA, Nakatsuji H, Caricato M, Li X, Hratchian HP, Izmaylov AF, Bloino J, Zheng G, Sonnenberg JL, Hada M, Ehara M, Toyota K, Fukuda R, Hasegawa J, Ishida M, Nakajima T, Honda Y, Kitao O, Nakai H, Vreven T, Montgomery JA Jr, Peralta JE, Ogliaro F, Bearpark M, Heyd JJ, Brothers E, Kudin KN, Staroverov VN, Keith T, Kobayashi R, Normand J, Raghavachari K, Rendell A, Burant JC, Iyengar SS, Tomasi J, Cossi M, Rega N, Millam JM, Klene M, Knox JE, Cross JB, Bakken V, Adamo C, Jaramillo J, Gomperts R, Stratmann RE, Yazyev O, Austin AJ, Cammi R, Pomelli C, Ochterski JW, Martin RL, Morokuma K, Zakrzewski VG, Voth GA, Salvador P, Dannenberg JJ, Dapprich S, Daniels AD, Farkas O, Foresman JB, Ortiz JV, Cioslowski J, Fox DJ (2009) Gaussian 09, revision A02. Gaussian Inc., Wallingford
56. Coropceanu V, Cornil J, da Silva Filho DA, Olivier Y, Silbey R, Bredas J-L (2007) Charge transport in organic semiconductors. Chem Rev 107(4):926–952. doi:10.1021/cr050140x
57. Valeev EF, Coropceanu V, da Silva Filho DA, Salman S, Brédas J-L (2006) Effect of electronic polarization on charge-transport parameters in molecular organic semiconductors. J Am Chem Soc 128(30): 9882–9886. doi:10.1021/ja061827h
58. Senthilkumar K, Grozema FC, Bickelhaupt FM, Siebbeles LDA (2003) Charge transport in columnar stacked triphenylenes: effects of conformational fluctuations on charge transfer integrals and site energies. J Chem Phys 119(18):9809–9817. doi:10.1063/1.1615476
59. te Velde G, Bickelhaupt FM, Baerends EJ, Guerra CF, Van Gisbergen SJA, Snijders JG, Ziegler T (2001) Chemistry with ADF. J Comput Chem 22(9):931–967. doi:10.1002/jcc.1056
60. Schein LB, McGhie AR (1979) Band-hopping mobility transition in naphthalene and deuterated naphthalene. Phys Rev B 20(4):1631–1639. doi:10.1103/PhysRevB.20.1631
61. Coropceanu V, Kwon O, Wex B, Kaafarani BR, Gruhn NE, Durivage JC, Neckers DC, Bredas JL (2006) Vibronic coupling in organic semiconductors: the case of fused polycyclic benzene-thiophene structures. Chem Eur J 12(7):2073–2080. doi:10.1002/chem.200500879
62. Yang X, Wang L, Wang C, Long W, Shuai Z (2008) Influences of crystal structures and molecular sizes on the charge mobility of organic semiconductors: oligothiophenes. Chem Mater 20(9):3205–3211. doi:10.1021/cm8002172
63. Nan G, Wang L, Yang X, Shuai Z, Zhao Y (2009) Charge transfer rates in organic semiconductors beyond first-order perturbation: from weak to strong coupling regimes. J Chem Phys 130(2):024704. doi:10.1063/1.3055519
64. Wex B, Kaafarani BR, Schroeder R, Majewski LA, Burckel P, Grell M, Neckers DC (2006) New organic semiconductors and their device performance as a function of thiophene orientation. J Mater Chem 16(12):1121–1124. doi:10.1039/b512191d
65. Bisquert J (2008) Interpretation of electron diffusion coefficient in organic and inorganic semiconductors with broad distributions of states. Phys Chem Chem Phys 10(22):3175–3194. doi:10.1039/b719943k
66. Perdew JP, Burke K, Ernzerhof M (1996) Generalized gradient approximation made simple. Phys Rev Lett 77(18):3865–3868. doi:10.1103/PhysRevLett.77.3865
67. Kresse G, Hafner J (1993) Ab initio molecular dynamics for liquid metals. Phys Rev B Condens Matter 47(1):558–561. doi:10.1103/PhysRevB.47.558

68. Kresse G, Hafner J (1994) Ab initio molecular-dynamics simulation of the liquid-metal-amorphous-semiconductor transition in germanium. Phys Rev B Condens Matter 49(20):14251–14269. doi:10.1103/PhysRevB.49.14251
69. Kresse G, Furthmüller J (1996) Efficiency of ab-initio total energy calculations for metals and semiconductors using a plane-wave basis set. Comp Mater Sci 6(1):15–50. doi:10.1016/0927-0256(96)00008-0
70. Blochl PE (1994) Projector augmented-wave method. Phys Rev B Condens Matter 50(24):17953–17979. doi:10.1103/PhysRevB.50.17953
71. Kresse G, Joubert D (1999) From ultrasoft pseudopotentials to the projector augmented-wave method. Phys Rev B 59(3):1758–1775. doi:10.1103/PhysRevB.59.1758
72. Pack JD, Monkhorst HJ (1977) "Special points for Brillouin-zone integrations"—a reply. Phys Rev B 16(4):1748–1749. doi:10.1103/PhysRevB.16.1748
73. Doi K, Yoshida K, Nakano H, Tachibana A, Tanabe T, Kojima Y, Okazaki K (2005) Ab initio calculation of electron effective masses in solid pentacene. J Appl Phys 98(11):113709. doi:10.1063/1.2138381
74. Zhu L, Yi Y, Li Y, Kim E-G, Coropceanu V, Bredas J-L (2012) Prediction of remarkable ambipolar charge-transport characteristics in organic mixed-stack charge-transfer crystals. J Am Chem Soc 134(4):2340–2347. doi:10.1021/ja210284s
75. Zhu L, Coropceanu V, Yi Y, Chilukuri B, Cundari TR, Brédas J-L (2013) Electronic and charge-transport properties of the $Au_3(CH_3N{=}COCH_3)_3$ crystal: a density functional theory study. J Phys Chem Lett 4(13):2186–2189. doi:10.1021/jz400950v
76. Chen X-K, Zou L-Y, Guo J-F, Ren A-M (2012) An efficient strategy for designing n-type organic semiconductor materials—introducing a six-membered imide ring into aromatic diimides. J Mater Chem 22(13):6471–6484. doi:10.1039/c2jm15935j
77. Wen S, Deng W-Q, Han K-L (2010) Ultra-low resistance at TTF-TCNQ organic interfaces. Chem Commun 46(28):5133–5135. doi:10.1039/c0cc00955e
78. Wang L, Nan G, Yang X, Peng Q, Li Q, Shuai Z (2010) Computational methods for design of organic materials with high charge mobility. Chem Soc Rev 39(2):423–434. doi:10.1039/b816406c
79. Hohenstein EG, Sherrill CD (2010) Density fitting and Cholesky decomposition approximations in symmetry-adapted perturbation theory: implementation and application to probe the nature of π–π interactions in linear acenes. J Chem Phys 132:184111. doi:10.1063/1.3426316
80. Hohenstein EG, Parrish RM, Sherrill CD, Turney JM, Schaefer HF (2011) Large-scale symmetry-adapted perturbation theory computations via density fitting and Laplace transformation techniques: investigating the fundamental forces of DNA–intercalator interactions. J Chem Phys 135:174107. doi:10.1063/1.3656681
81. Lu T, Chen F (2012) Multiwfn: A multifunctional wavefunction analyzer. J Comput Chem 33(5):580–592. doi:10.1002/jcc.22885
82. Lu T, Chen F (2012) Quantitative analysis of molecular surface based on improved marching tetrahedra algorithm. J Mol Graph Model 38(0):314–323. doi:10.1016/j.jmgm.2012.07.004
83. Zhang S-F, Chen X-K, Fan J-X, Ren A-M (2013) Charge transport properties in a series of five-ring-fused thienoacenes: a quantum chemistry and molecular mechanic study. Org Electron 14(2):607–620. doi:10.1016/j.orgel.2012.12.001
84. Tang X-D, Liao Y, Geng H, Shuai Z-G (2012) Fascinating effect of dehydrogenation on the transport properties of N-heteropentacenes: transformation from p- to n-type semiconductor. J Mater Chem 22(35):18181–18191. doi:10.1039/c2jm33039c
85. Fratini S, Ciuchi S (2009) Bandlike motion and mobility saturation in organic molecular semiconductors. Phys Rev Lett 103(26):266601. doi:10.1103/PhysRevLett.103.266601
86. Sanchez-Carrera RS, Paramonov P, Day GM, Coropceanu V, Bredas J-L (2010) Interaction of charge carriers with lattice vibrations in oligoacene crystals from naphthalene to pentacene. J Am Chem Soc 132(41):14437–14446. doi:10.1021/ja1040732
87. Hummer K, Ambrosch-Draxl C (2005) Electronic properties of oligoacenes from first principles. Phys Rev B 72(20):205205. doi:10.1103/Physrevb.72.205205
88. de Wijs GA, Mattheus CC, de Groot RA, Palstra TTM (2003) Anisotropy of the mobility of pentacene from frustration. Synthetic Met 139(1):109–114. doi:10.1016/s0379-6779(03)00020-1
89. Li Y, Coropceanu V, Bredas JL (2012) Thermal narrowing of the electronic bandwidths in organic molecular semiconductors: impact of the crystal thermal expansion. J Phys Chem Lett 3(22):3325–3329. doi:10.1021/Jz301575u
90. Wang L, Li Q, Shuai Z, Chen L, Shi Q (2010) Multiscale study of charge mobility of organic semiconductor with dynamic disorders. Phys Chem Chem Phys 12(13):3309–3314. doi:10.1039/b913183c
91. Bunte SW, Sun H (2000) Molecular modeling of energetic materials: the parameterization and validation of nitrate esters in the COMPASS force field. J Phys Chem B 104(11):2477–2489. doi:10.1021/jp991786u
92. Li Y, Yi YP, Coropceanu V, Bredas JL (2012) Symmetry effects on nonlocal electron–phonon coupling in organic semiconductors. Phys Rev B 85(24):245201. doi:10.1103/Physrevb.85.245201
93. Huang J-D, Wen S-H, Deng W-Q, Han K-L (2011) Simulation of hole mobility in alpha-oligofuran crystals. J Phys Chem B 115(10):2140–2147. doi:10.1021/jp108125q
94. Nan G, Li Z (2012) Phase dependence of hole mobilities in dibenzo-tetrathiafulvalene crystal: a first-principles study. Org Electron 13(7):1229–1236. doi:10.1016/j.orgel.2012.03.033
95. Chua LL, Zaumseil J, Chang JF, Ou ECW, Ho PKH, Sirringhaus H, Friend RH (2005) General observation of n-type field-effect behaviour in organic semiconductors. Nature 434(7030):194–199. doi:10.1038/nature03376